Quantitative conformational profiling of kinase inhibitors reveals origins of selectivity for Aurora kinase activation states

Eric W. Lake[a], Joseph M. Muretta[b], Andrew R. Thompson[b], Damien M. Rasmussen[b], Abir Majumdar[a], Erik B. Faber[c], Emily F. Ruff[a], David D. Thomas[b], and Nicholas M. Levinson[a,d,1]

[a]Department of Pharmacology, University of Minnesota, Minneapolis, MN 55455; [b]Department of Biochemistry, Molecular Biology, and Biophysics, University of Minnesota, Minneapolis, MN 55455; [c]Department of Medicinal Chemistry, University of Minnesota, Minneapolis, MN 55455; and [d]Masonic Cancer Center, University of Minnesota, Minneapolis, MN 55455

Edited by Kevan M. Shokat, University of California, San Francisco, CA, and approved November 7, 2018 (received for review June 28, 2018)

Protein kinases undergo large-scale structural changes that tightly regulate function and control recognition by small-molecule inhibitors. Methods for quantifying the conformational effects of inhibitors and linking them to an understanding of selectivity patterns have long been elusive. We have developed an ultrafast time-resolved fluorescence methodology that tracks structural movements of the kinase activation loop in solution with angstrom-level precision, and can resolve multiple structural states and quantify conformational shifts between states. Profiling a panel of clinically relevant Aurora kinase inhibitors against the mitotic kinase Aurora A revealed a wide range of conformational preferences, with all inhibitors promoting either the active DFG-in state or the inactive DFG-out state, but to widely differing extents. Remarkably, these conformational preferences explain broad patterns of inhibitor selectivity across different activation states of Aurora A, with DFG-out inhibitors preferentially binding Aurora A activated by phosphorylation on the activation loop, which dynamically samples the DFG-out state, and DFG-in inhibitors binding preferentially to Aurora A constrained in the DFG-in state by its allosteric activator Tpx2. The results suggest that many inhibitors currently in clinical development may be capable of differentiating between Aurora A signaling pathways implicated in normal mitotic control and in melanoma, neuroblastoma, and prostate cancer. The technology is applicable to a wide range of clinically important kinases and could provide a wealth of valuable structure–activity information for the development of inhibitors that exploit differences in conformational dynamics to achieve enhanced selectivity.

protein kinases | Aurora inhibitors | conformational selectivity | DFG motif

Protein kinases play central roles in signal transduction pathways controlling the growth and proliferation of eukaryotic cells, and mutated protein kinases are a major cause of human cancer. The advent of targeted kinase inhibitors like imatinib, which blocks the BCR-Abl kinase that causes chronic myeloid leukemia (1), and erlotinib, which targets mutated epidermal growth factor receptor in lung cancer (2, 3), has substantially changed the landscape of modern cancer therapy. As of 2018, 37 kinase inhibitors have received regulatory approval for the treatment of cancer and autoimmune disease, and hundreds are in clinical and preclinical development.

A substantial challenge encountered in the development of ATP-competitive kinase inhibitors is obtaining sufficient specificity for the target kinase, a consequence of the high degree of conservation in the active site among the >500 members of the kinase superfamily (4). Early crystallographic studies (5–7) clarified that the conformational plasticity of the kinase domain plays a role in determining inhibitor selectivity, and led to the classification of inhibitors into two general types. Type I inhibitors are thought to either recognize the active state or bind without regard to the conformation of the kinase, whereas type II inhibitors specifically recognize inactive states in which a catalytically important Asp–Phe–Gly (DFG) motif, located on the flexible activation loop of the kinase, is flipped relative to its orientation in the active state (referred to as "DFG-out," in contrast to the active "DFG-in" state). The observation that the inactive DFG-out states of kinases are more divergent than the catalytically competent DFG-in state has led to a focus on type II inhibitors as a potential answer to the selectivity problem (8, 9). However, kinome-wide profiling of kinase inhibitors has revealed that selectivity patterns are complex, and while type II compounds do seem to be more selective on average, there are numerous examples of highly selective type I inhibitors and relatively nonselective type II inhibitors (10, 11). A quantitative understanding of the mechanistic connections between binding mode, conformational change, and selectivity is an important missing piece of the puzzle for the rational design of selective kinase inhibitors. Here, we develop an experimental approach to address this challenge and apply it to understanding the conformational effects of inhibitors of Aurora kinase A.

Aurora A (AurA) is a member of the Aurora family of serine/threonine kinases that play central roles in mitosis (12). AurA exists in multiple functionally and spatially distinct pools in mitotic cells, with a pool localized to centrosomes controlling

Significance

Many drugs trigger changes to the structure of their target receptor upon binding. These conformational effects are thought to be an essential part of molecular recognition but have proven challenging to quantify. Using a high-throughput method for tracking structural changes in a protein kinase in solution, we discovered that many clinically important cancer drugs trigger substantial structural changes to their target protein kinase Aurora A, and that these effects systematically account for the ability of the drugs to differentiate between different biochemical forms of Aurora A. The results provide insight into mechanisms of drug selectivity and suggest strategies for tailoring inhibitors to target certain cancers in which Aurora A has been dysregulated in different ways.

Author contributions: E.W.L., E.F.R., D.D.T., and N.M.L. designed research; E.W.L., A.R.T., D.M.R., A.M., E.B.F., and N.M.L. performed research; E.W.L., J.M.M., A.R.T., E.F.R., D.D.T., and N.M.L. contributed new reagents/analytic tools; E.W.L., J.M.M., A.R.T., D.M.R., A.M., and N.M.L. analyzed data; and E.W.L. and N.M.L. wrote the paper.

Conflict of interest statement: A nonprovisional patent application covering the design and implementation of the FRET sensor screening technology was submitted to the US Patent and Trademark Office in September 2017 and is currently pending (PCT/US17/50608). The authors on this application are N.M.L., J.M.M., E.F.R., D.D.T., and E.W.L.

This article is a PNAS Direct Submission.

[1]To whom correspondence should be addressed. Email: nml@umn.edu.

This article contains supporting information online at www.pnas.org/lookup/suppl/doi:10.1073/pnas.1811158115/-/DCSupplemental.

Published online December 5, 2018.

centrosome maturation and mitotic entry (13–15), and a pool localized to spindle microtubules promoting nucleation of microtubules by chromatin and construction of the bipolar mitotic spindle (16, 17). AurA also performs other important cellular functions through the formation of complexes with regulatory proteins, including the oncogenic transcription factors c-Myc and N-Myc (18, 19). The discovery that both AurA and its closely related family member Aurora B (AurB) are amplified in a variety of solid tumors (20, 21) motivated the development of a large number of Aurora kinase inhibitors, many of which are in clinical trials, but as yet no Aurora inhibitors have received regulatory approval.

Each cellular pool of AurA is regulated by different protein–protein interactions and posttranslational modifications. Activation of AurA at centrosomes occurs through autophosphorylation of a threonine residue (T288) in the activation loop (22, 23), whereas activation of AurA on spindle microtubules is driven by complex formation with the spindle assembly factor Tpx2 (24, 25). The conformational dynamics of AurA are tuned in different ways upon activation by phosphorylation or Tpx2 binding (26–29), suggesting that each functional pool in cells possesses distinct conformational properties that will modulate the interactions with inhibitors, impacting efficacy in a tumor context-specific fashion. Recent studies have reported connections between AurA dynamics and inhibitor recognition in individual cases (27, 30), but a broad mechanistic understanding is lacking. Here, we present a comprehensive study of the conformational effects of Aurora kinase inhibitors across different activation states of AurA and show that all inhibitors, including type I and type II compounds, cause substantial structural changes upon binding, and that these effects interact with the conformational ensemble of the kinase to determine binding selectivity. The results have implications for the therapeutic application of Aurora inhibitors in different patient populations and suggest that a broad utilization of this approach could substantially aid the development of kinase inhibitors with improved selectivity.

Results

AurA Activation States Provide Multiple Baselines for Tracking Inhibitor-Driven Structural Changes. To monitor the conformational state of AurA in a high-throughput format, we built a Förster resonance energy transfer (FRET) sensor that tracks the position of the activation loop of the kinase (Fig. 1 *A* and *B*) and coupled it with a state-of-the-art fluorescence lifetime plate reader based on direct waveform recording technology (31), which permits rapid nanosecond fluorescence lifetime measurements in multiwell plates with signal-to-noise ratios up to 1,000 (Fig. 1*C*). The FRET sensor uses donor and acceptor dyes incorporated by site-specific labeling onto the mobile activation loop of AurA and a static reference point on a distal surface of the kinase, with the DFG-out state yielding high FRET (shorter donor–acceptor distance, shorter lifetime) and the DFG-in state yielding low FRET (longer donor–acceptor distance, longer lifetime) (Fig. 1 *A* and *B*). Lifetime data were analyzed by fitting to a structural model in which the decrease in the donor lifetime in the presence of acceptor is accounted for by a Gaussian distribution of interfluorophore distances, representing the conformational ensemble in solution (Fig. 1*D* and *SI Appendix*). In this model, a change in distance can arise either from a shift in the equilibrium between two structural states or from the adoption of a new structural state.

Since Tpx2 binding and phosphorylation on T288 have been shown to differentially affect the conformational dynamics of AurA (26–28), we reasoned that patterns of inhibitor-induced conformational changes may differ across the different activation states of the enzyme. We therefore used our time-resolved (TR)-FRET assay to probe the conformational dynamics of AurA in four biochemical states possessing different levels of catalytic activity and representing different cellular pools of the kinase: (*i*) unphosphorylated AurA ("*Unphos*"; inactive), (*ii*) phosphorylated AurA ("*Phos*"; active, centrosomal pool), (*iii*) unphosphorylated AurA bound to Tpx2 ("*Unphos+Tpx2*"; active, spindle pool), and (*iv*) phosphorylated AurA bound to Tpx2 ["*Phos+Tpx2*"; highly active, spindle pool in melanoma cells (32)]. The TR-FRET analysis resolved all four biochemical states with high confidence (*SI Appendix*, Fig. S1*F*) and consistency (Fig. 1 *D* and *E*). The data confirm previous reports (26) that the DFG-out state is favored in the isolated kinase regardless of phosphorylation, observed as broad distance distributions centered at 35.8 ± 0.2 and 39.8 ± 0.2 Å for the *Unphos* and *Phos* states, respectively, and that the binding of Tpx2 triggers a conformational change to the DFG-in state,

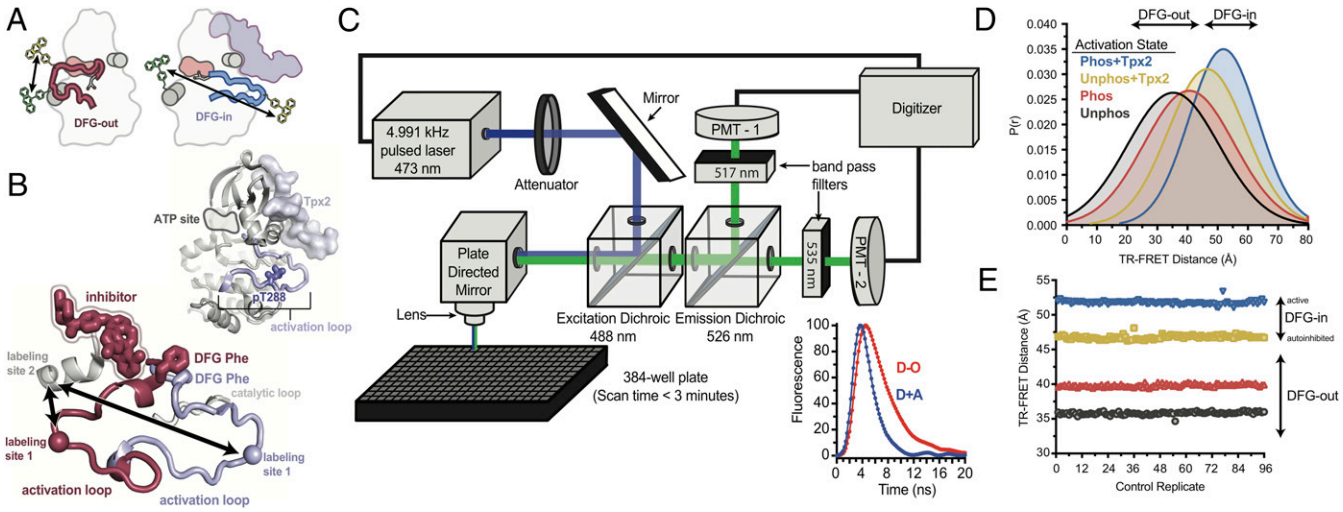

Fig. 1. Activation states of AurA define four conformational baselines for assessing effects of inhibitor binding. (*A*) Schematics of the TR-FRET labeling scheme showing the positions of the two fluorescent dyes on the activation loop and αD-helix in the active (*Right*) and inactive (*Left*) states. (*B*) The conformation of the activation loop is shown for active AurA bound to Tpx2 (blue; PDB ID code 1OL5) and AurA bound to a DFG-out inhibitor (magenta; PDB ID code 3H10), with the dye labeling sites shown as spheres. The *Upper Inset* shows the full structure of the kinase domain bound to Tpx2 with the T288 phosphorylation site indicated. (*C*) Layout of the nanosecond time-resolved fluorescence plate reader used for TR-FRET experiments. The *Lower Inset* shows example waveforms for donor-plus-acceptor (D+A) and donor-only (D-O) labeled protein. (*D*) Average Gaussian distance distributions obtained for the four activation states of AurA, inactive unphosphorylated AurA (black), phosphorylated AurA (red), unphosphorylated AurA bound to Tpx2 (yellow), and phosphorylated AurA bound to Tpx2 (blue). The approximate distance ranges corresponding to DFG-in and DFG-out states are indicated for reference. (*E*) TR-FRET distances measured for the four activation states of AurA across 96 replicate experiments in 384-well plates.

observed as a shift of the distribution to a longer distance (46.8 ± 0.3 Å) and a narrower width in the *Unphos+Tpx2* state. The phosphorylation-driven conformational switch in the activation loop, in which the loop transitions from an autoinhibited DFG-in substate to an active DFG-in substate (28), is also apparent in the data as an additional increase in the FRET distance going from the *Unphos+Tpx2* to the *Phos+Tpx2* state (51.7 ± 0.3 Å; Fig. 1*E*) and a further decrease in the width of the distribution.

The TR-FRET data highlight that the distinct effects of phosphorylation and Tpx2 binding lead to unique conformational properties for each activation state of the kinase, with a progressive shift toward the DFG-in state and reduction in conformational plasticity going from the *Unphos* state to the *Phos+Tpx2* state. These results establish four different conformational baselines from which to analyze the effects of inhibitor binding.

Aurora Inhibitors Exhibit Three Classes of Conformational Behavior. We used the TR-FRET assay to define the conformational effects of a set of 24 commercially available Aurora kinase inhibitors on each of the four biochemical states of AurA (Fig. 2*A*). This diverse inhibitor set encompasses a variety of chemical scaffolds (*SI Appendix*, Fig. S2) and a broad range of molecular weights (*SI Appendix*, Table S1), and includes examples of DFG-in and DFG-out inhibitors as classified by X-ray structures. While some of the inhibitors were developed to target other kinases, all of them exhibit nanomolar or lower binding affinity for AurA. The majority of the compounds have been tested in clinical trials, and several are still in clinical development (Fig. 2*A*), with more than a dozen ongoing trials of alisertib in a variety of cancers.

Fluorescence lifetime waveforms were recorded for titrations of each compound from 1 nM to 5 μM in 384-well assay plates. Inhibitor-induced conformational changes were readily apparent in the fluorescence emission waveforms, with the donor-plus-acceptor samples showing substantial binding-induced changes in lifetime (*SI Appendix*, Fig. S3 *A* and *B*). Fitting of the lifetime data revealed a rich diversity of inhibitor-induced conformational changes. Conformational shifts occurred in both directions (toward DFG-in and toward DFG-out), varied in magnitude from relatively small to as large as those observed with Tpx2, and changed in consistent ways across the biochemical states of the kinase. The most dramatic changes were observed with SNS-314, which triggered a nearly complete switch to the DFG-in conformation in the *Unphos* and *Phos* states, and AMG-900, which caused the largest shift to the DFG-out state in the *Phos+Tpx2* state.

Three qualitatively distinct classes of conformational behavior were observed in the TR-FRET dataset: (*i*) partial increases in FRET distance, consistent with equilibrium shifts toward the DFG-in state; (*ii*) partial decreases in distance in all biochemical states, consistent with equilibrium shifts toward the DFG-out state; and (*iii*) complete switches to new FRET distances that were characteristic for a given inhibitor, consistent with induction of unique structural states (Fig. 2*B* and *SI Appendix*, Fig. S4). These three classes correspond, with one informative exception, to (*i*) type I inhibitors that promote the DFG-in state, (*ii*) type I inhibitors that promote the DFG-out state, and (*iii*) type II inhibitors.

A

Inhibitor	Clinical Trials	Aurora-family [a] selectivity	Other [a] targets	DFG-in/out by x-ray	DFG-in/out this study
AT-9283	Phase 2 (multiple myeloma)	pan	JAK2/3, ABL	both	in (medium)
CCT-129202	preclinical	pan			in (medium)
CCT-137690	preclinical	pan		in	in (medium)
CYC-116	Phase 1 (solid tumors)	pan	FLT3, VEGFR	in	in (medium)
ENMD-2076	Phase 2 (FLC, STS,TNBC, OC)	AurA	FLT3, RET		in (medium)[b]
hesperadin	preclinical	AurB		in	in (medium)
JNJ-7706621	preclinical	pan	CDKs	in	in (weak)
KW-2449	Phase 1 (AML)	pan	ABL, FLT3		in (medium)
PF-03814735	Phase 1 (solid tumors)	pan	FLT1, FAK	in	in (medium)
PHA-680632	preclinical	pan		out	in (medium)
reversine	preclinical	pan		in	in (medium)
SNS-314	Phase 1 (solid tumors)	pan	TrkB	in	in (strong)
TAE-684	preclinical	AurA	ALK	in	in (medium)
TAK-901	Phase 1 (solid tumors)	pan	FLT3		in (medium)
danusertib	Phase 2 (CML, prostate cancer)	pan	ABL, RET	both	out (type I)
MLN-8054	Phase 1	AurA	DRAK2	out	out (type I)
alisertib	Phase 2 (SCLC, NB, NEPC, NHL)	AurA			out (type I)
VX-680	Phase 2 (CML, solid tumors)	pan	ABL, FLT3	both	out (type I)
AMG-900	Phase 1 (AML, solid tumors)	pan	DDR1,2	out	out (type II)
BI-847325	Phase 1 (solid tumors)	pan	MEK1,2	in	out (type II)
GSK-1070916	Phase 1 (solid tumors)	AurB	FLT1		out (type II)
MK-5108	Phase 1 (solid tumors)	AurA	TrkA, ABL	out	out (type I)
MK-8745	preclinical	AurA			out (type I)
ZM-447439	preclinical	pan		in	out (type II)

[a]data from Selleckchem.com
[b]weak for Unphos

AML, acute myeloid leukemia
NEPC, neuroendocrine prostate cancer
SCLC, small cell lung cancer
CML, chronic myeloid leukemia
NHL, non-hodgkin lympoma
STS, soft-tissue sarcoma
FLC, fibrolamellar carcinoma
OC, ovarian cancer
TNBC, triple-negative breast cancer
NB, neuroblastoma

B

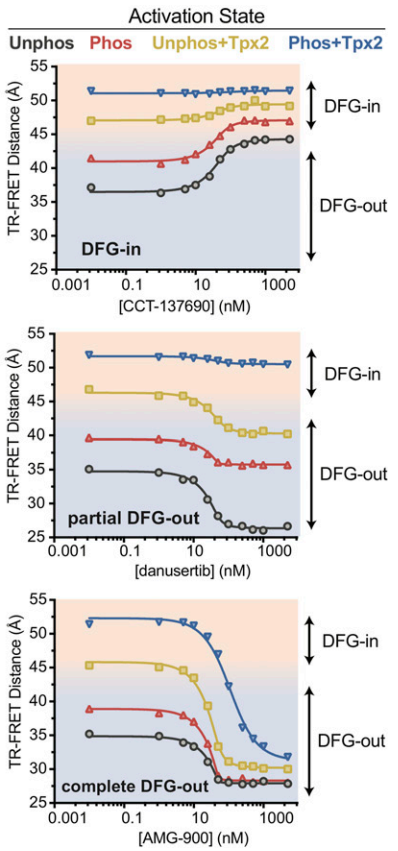

Fig. 2. TR-FRET analysis identifies three classes of conformational effects among existing AurA inhibitors. (*A*) The table shows collated data for the 24 AurA inhibitors analyzed in this study. Trial data were taken from ClinicalTrials.gov, selectivity data from commercial inhibitor vendors, and structural data from the Protein Data Bank. The table is broken into sections corresponding to the three classes of conformational effects described in this study. (*B*) Representative TR-FRET binding curves for the three inhibitor classes that induce DFG-in shifts (*Top*), partial DFG-out shifts (*Middle*), and complete DFG-out shifts (*Bottom*), measured for all activation states of AurA. Background shading represents the approximate DFG-in (pale orange) and DFG-out (pale blue) regions. Similar curves are shown for all inhibitors in *SI Appendix*, Fig. S4.

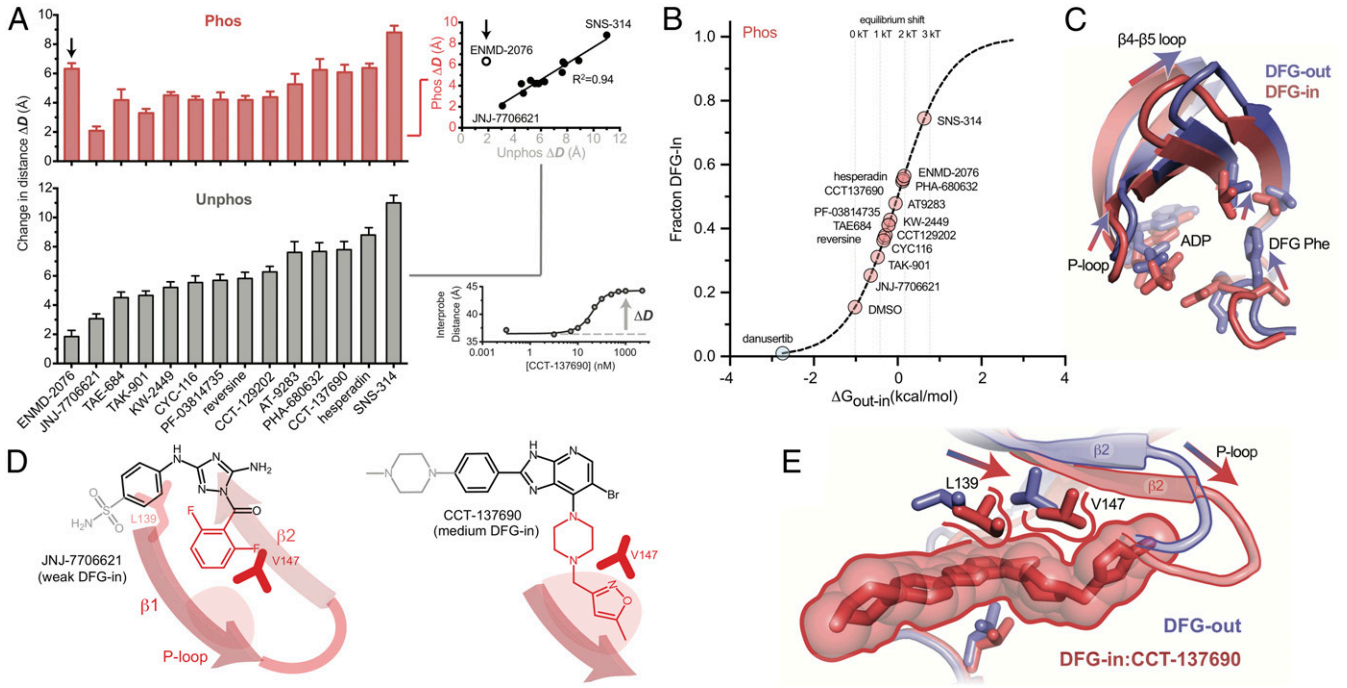

Fig. 3. Type I inhibitors stabilize the DFG-in state by promoting closure of the active site cleft. (*A*) Histograms of the TR-FRET distance changes (Δ*D*, illustrated in *Bottom Right Inset*) observed for the 14 DFG-in inducers binding to the *Unphos* and *Phos* biochemical states of AurA. Data represent values and 95% confidence intervals derived from fitting individual TR-FRET binding curves (the curves are shown in *SI Appendix*, Fig. S4*A*). The *Inset* shows the correlation of the Δ*D* values for the *Unphos* and *Phos* states, highlighting ENMD-2076 as an exception. (*B*) The DFG-in mole fractions derived from a two-Gaussian distance fit (*SI Appendix*) are plotted against the inferred free energy difference between DFG-in and DFG-out states for the phosphorylated kinase. Inclusion of the DFG-out inhibitor danusertib in the fitting analysis was necessary to establish the baseline mole fraction of apo AurA, which is in equilibrium between DFG-in and DFG-out states. The dashed vertical lines indicate changes in the DFG equilibrium of integer values of kT. (*C*) Crystal structures of AurA bound to ADP in the DFG-in (red; PDB ID code 1OL5) and DFG-out (blue; PDB ID code 5L8K) states aligned on the C-terminal lobe, highlighting the opening of the active-site cleft in the DFG-out state. (*D*) Chemical structures of a representative medium-strength DFG-in inducer (CCT-137690) and the weakest DFG-in inducer (JNJ-7706621), with the hinge-binding motif colored black, and the P-loop binding substituents red. The β-strands of the P-loop are shown in red, and the pocket bounded by V147 is shown in faint pink. Structures of all DFG-in inducers colored in the same fashion are shown in *SI Appendix*, Fig. S5. (*E*) Crystal structures of AurA in the DFG-out state (blue; PDB ID code 5L8K) and in the DFG-in state bound to the DFG-in inducer CCT-137690 (red; PDB ID code 2X6E), highlighting the positioning of the 5-methyl-isoxazole group in the pocket beyond V147, and the ratcheting of the P-loop into a closed conformation. X-ray structures or docking poses for the other DFG-in inducers are shown in *SI Appendix*, Fig. S5.

The Majority of Type I Inhibitors Stabilize the DFG-In State by Promoting Active Site Closure. Fourteen of the compounds in our dataset promoted the DFG-in conformation across biochemical states of AurA, albeit to widely varying extents (*SI Appendix*, Fig. S4*A*). Across inhibitors, the conformational shifts were largest for the *Unphos* and *Phos* states (Fig. 3*A*), and more modest for the *Unphos+Tpx2* and *Phos+Tpx2* states, where the DFG-in state already predominates. The magnitudes of the shifts for the *Phos* and *Unphos* states were strongly correlated, with the notable exception of ENMD-2076, which caused a larger shift in the *Phos* state than the *Unphos* state (Fig. 3*A*, *Upper Right Inset*), suggesting that it preferentially recognizes the active DFG-in substate promoted by phosphorylation (28).

These overall trends are consistent with a simple shift of the preexisting DFG equilibrium present in the apo kinase. This hypothesis was tested by fitting the lifetime data to a two-state model in which the DFG-out and DFG-in states are represented by separate Gaussian distance distributions, which are globally shared across all 14 compounds, while the mole fractions of each state are allowed to vary by compound (*SI Appendix*). For both the *Unphos* and *Phos* states, the mole fractions were consistent with shifts derived from the single-distance fits, but probing the populations allows the conformational effects to be expressed on an energetic scale (Fig. 3*B*). This analysis showed that the strongest DFG-in inducer, SNS-314, alters the DFG equilibrium by ~2 kcal/mol, and that most of the other inhibitors shift the equilibrium by 0.5 to 1.5 kcal/mol.

Cocrystal structures are available for 10 of the DFG-in inducers (*SI Appendix*, Fig. S5*A*). Among these, only SNS-314 reaches into the back of the ATP-binding site, where it makes extensive contacts with the DFG-motif and forms a hydrogen bond network with residue E181 of the αC-helix (*SI Appendix*, Fig. S5*B*), explaining its strong preference for the DFG-in state (33). The structural data for the other inhibitors reveal little or no interaction between the inhibitors and the DFG motif. For the four inhibitors for which no X-ray structures are available (ENMD-2076, KW2449, TAK-901, and CCT-129202), we performed molecular docking to model their interactions with the active site (*SI Appendix*) and found that these inhibitors also appear not to directly contact the DFG motif (*SI Appendix*, Fig. S5*C*). These structural observations raised the question of why effects on the DFG equilibrium were so pervasive among these type I inhibitors.

X-ray structures show that the N- and C-terminal lobes of AurA are more separated, and the active site more open, in the DFG-out state than the DFG-in state (24, 34). This can be attributed to the phenylalanine sidechain of the DFG motif (F275), which flips up against the N-terminal lobe in the DFG-out state, prying the lobes apart (Fig. 3*C*). Structures of the kinase bound to nucleotides show that, when the active site opens, nucleotide remains bound to the N-terminal lobe and dissociates from the base of the active site formed by the C-terminal lobe, weakening the interaction between the nucleotide and the active site. This explains previous reports that nucleotide binding to AurA leads to a population shift toward the DFG-in state (26, 28) and suggests a possible mechanism by which inhibitors might also promote the

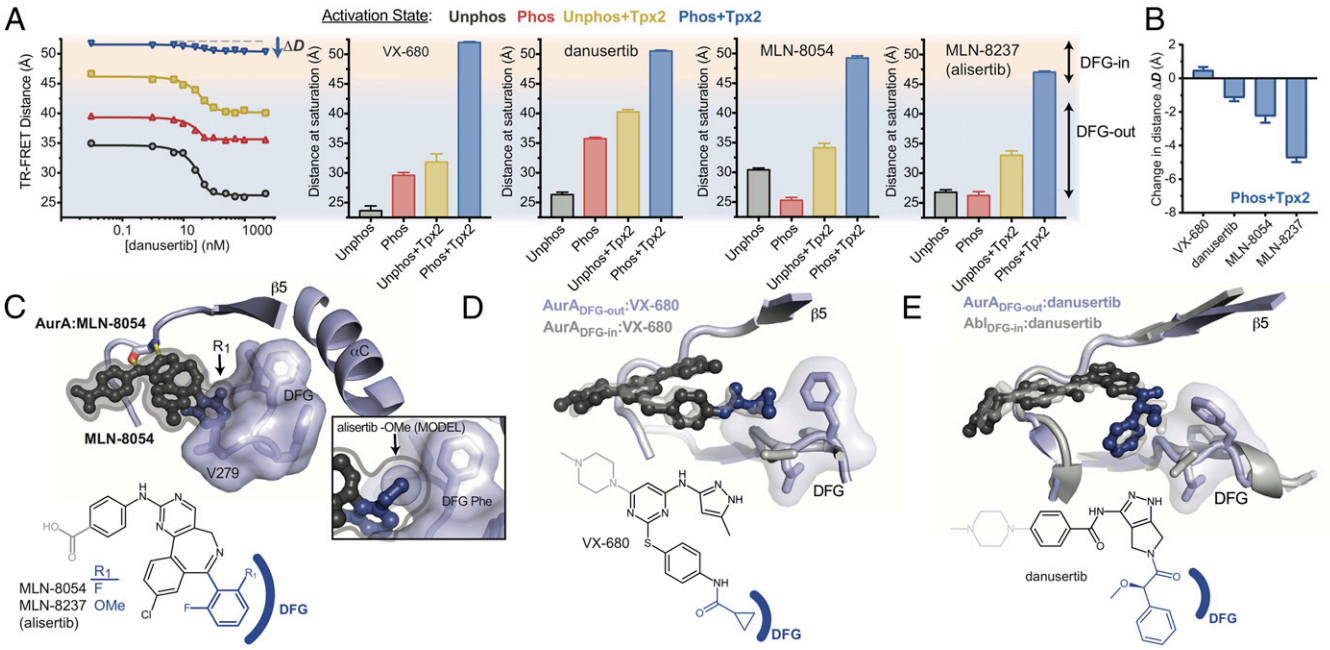

Fig. 4. Tpx2 overrides the conformational effects of most type I DFG-out inhibitors. (*A*, *Left*) Representative TR-FRET titration curves for danusertib, and (*Right*) histograms of the FRET distances reached upon saturation with each inhibitor, highlighting the variation across AurA activation states. The background shading represents the DFG-in (pale orange) and DFG-out (pale blue) regions of the TR-FRET analysis. Data represent the saturation points and 95% confidence intervals from fitting individual TR-FRET binding curves (the binding curves are shown in *SI Appendix*, Fig. S4*B*). (*B*) Inhibitor-induced changes in distance (Δ*D*) for phosphorylated AurA bound to Tpx2, highlighting the different degrees to which the inhibitors promote the DFG-out state in the presence of Tpx2. (*C*) Chemical structures of MLN-8054 and alisertib and X-ray structure of MLN-8054 bound to AurA (PDB ID code 2WTV). The *Inset* shows a model of alisertib bound to AurA, highlighting the likely positioning of the methoxy group of alisertib against the phenylalanine of the DFG motif. (*D*) Chemical structure of VX-680 and X-ray structures of VX-680 bound to AurA in the DFG-out state (blue; PDB ID code 4JBQ) and DFG-in state (gray; PDB ID code 3E5A). (*E*) Chemical structure of danusertib and X-ray structures of danusertib bound to AurA in the DFG-out state (blue; PDB ID code 2J50) and bound to Abl in the DFG-in state (gray; PDB ID code 2V7A).

DFG-in state. Inspection of the X-ray structures and docking poses reveals that a common feature of the DFG-in inhibitors is the positioning of substituents into a pocket under the phosphate-binding loop (P-loop) of the kinase (Fig. 3*D* and *SI Appendix*, Fig. S5 *A* and *C*) formed by the side chain of the P-loop residue V147, the backbone of the P-loop, and the aliphatic portion of the catalytic lysine residue K162 (Fig. 3*E*). Of note, the inhibitor with the smallest conformational shift, JNJ-7706621, contacts the V147 side chain but does not reach into the pocket beyond it (Fig. 3*D*) (35). These observations are consistent with a model in which inhibitors can promote the DFG-in state indirectly by ratcheting the active site closed through interactions with the P-loop and other features of the active site distal to the DFG motif.

Tpx2 Can Override the Conformational Effects of Type I DFG-Out Inhibitors. Four of the inhibitors in our dataset caused partial shifts toward the DFG-out state, resulting in each biochemical state of AurA yielding different observed FRET distances upon saturation with a given inhibitor (Fig. 4*A* and *SI Appendix*, Fig. S4*B*). These inhibitors triggered nearly complete DFG-out shifts when binding to the more flexible biochemical states (*Unphos*, *Phos*), but in the presence of Tpx2 the shifts were less complete and varied in magnitude among the different compounds (Fig. 4*B*), reflecting the opposing effects of Tpx2 and the inhibitors on the DFG equilibrium. The relative magnitudes of the shifts observed in the *Phos+Tpx2* state indicate that VX-680 and danusertib are the weakest DFG-out inducers, MLN-8054 is stronger, and its analog alisertib is the strongest (Fig. 4*B*).

The chemical structures of these inhibitors resemble those of type I inhibitors like the DFG-in inducers described above. MLN-8054 and alisertib are nonetheless known to have DFG-out binding modes based on the X-ray structure of MLN-8054 bound to AurA (Fig. 4*C*) (36). However, VX-680 and danusertib, which are dual Aurora/Abl kinase inhibitors that have been in clinical trials for imatinib-resistant chronic myeloid leukemia (37, 38), have been crystallized bound to a variety of kinases in both the DFG-in and DFG-out states (39–42) (Fig. 4 *D* and *E*). The TR-FRET data clarify that all four of these inhibitors promote DFG-out states in AurA, but to a limited extent that is largely overridden when the kinase is restrained in the DFG-in state by Tpx2 and phosphorylation. The X-ray data also suggest that the degree of stabilization of the DFG-out state is related to the extent of direct contacts between the inhibitor and the DFG motif, as VX-680 and danusertib make only superficial contacts with the DFG motif (Fig. 4 *D* and *E*) whereas MLN-8054 forms more extensive interactions (Fig. 4*C*). In alisertib, the substitution of a 2-methoxy group on the DFG-contacting aromatic ring for the 2-fluorine group of MLN-8054 would be expected to further increase the interface with the DFG phenylalanine (Fig. 4*C*, *Lower Right Inset*), presumably explaining why this inhibitor causes the largest DFG-out shift.

Interestingly, the chemical structure of danusertib is very similar to that of PHA-680632, which our data show promotes the DFG-in state. Comparison of the X-ray structures of danusertib and PHA-680632 bound to AurA revealed that despite very similar binding modes the diethylphenyl ring of PHA-680632 projects into the P-loop pocket, whereas the corresponding aromatic group of danusertib instead projects down into the C-terminal lobe, consistent with our model that engagement of the P-loop pocket is a key driver of DFG-in selectivity (*SI Appendix*, Fig. S6*A*).

Type II Inhibitors and a Special Class of Type I Inhibitor Trigger Complete DFG-Out Shifts Across AurA Activation States. Six of the inhibitors in our dataset induced characteristic FRET distances regardless of which biochemical form of AurA they bound to (Fig. 5*A*). This pattern contrasts with the partial shifts caused by the type I DFG-out inhibitors discussed above and suggests induction of unique structural states that differ from the DFG-in and DFG-out states of apo AurA (Fig. 5*A* and *SI Appendix*, Fig. S4*C*).

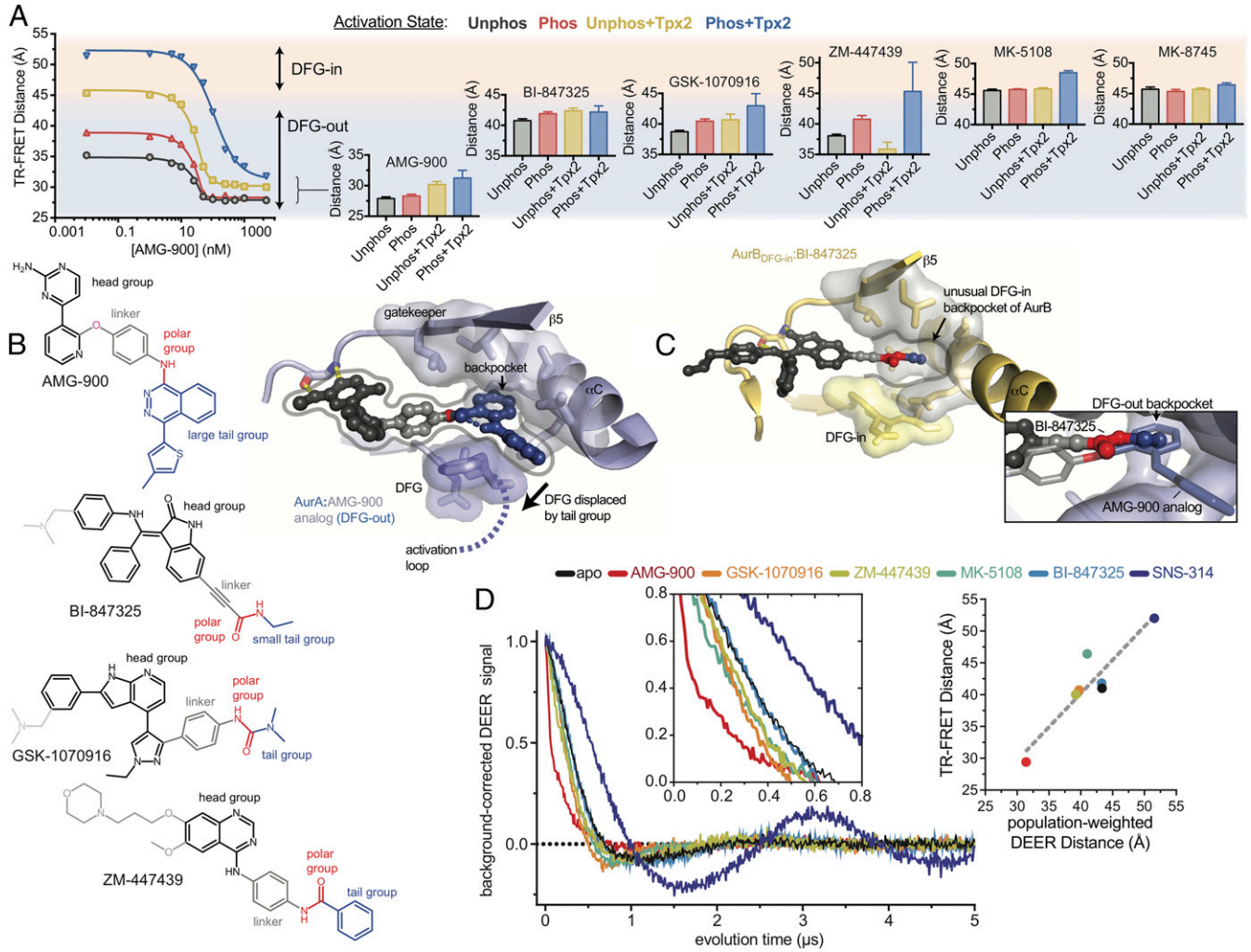

Fig. 5. Type II and a special class of type I inhibitors induce a complete switch to the DFG-out state. (*A*, *Left*) Representative TR-FRET titration curves for AMG-900, and (*Right*) histograms of the FRET distances reached upon saturation with each inhibitor, with background coloring as in Fig. 4. The *y* axes of the histograms are aligned with the *y* axis of the AMG-900 titration plot on the *Left*, and the data represent the saturation points and 95% confidence intervals from fitting individual TR-FRET binding curves (binding curves are shown in full in *SI Appendix*, Fig. S4*C*). (*B*) Chemical structures of the type II DFG-out compounds (*Left*) and X-ray structure of an analog of AMG-900 bound to AurA (*Top Right*) showing a classical type II binding mode (PDB ID code 3O51). The head groups of the inhibitors that engage the hinge region of the kinase are colored black; the linkers, gray; hydrogen bonding groups, red; and the hydrophobic tail groups that occupy the back pocket of the kinase, dark purple. Solubilizing groups are colored light gray. (*C*) X-ray structure of BI-847325 bound to AurB in the DFG-in state, with the occupied back pocket of AurB, usually occluded in the DFG-in state, highlighted (PDB ID code 5EYK). The *Inset* shows the AurB:BI-847325 structure aligned on the AurA:AMG-900 analog structure, highlighting the similar positioning of the hydrophobic tail groups of the two compounds in the back pocket of the DFG-out state. (*D*) Background-corrected DEER spectra of phosphorylated AurA bound to each of the four putative type II inhibitors, MK-5108 or SNS-314. The *Left Inset* shows an expanded view of the echo decays at short evolution time, which reflect the average spin–spin distances. The population-weighted average DEER distances are plotted against the corresponding TR-FRET distances in the *Right Inset*. A comparison of Tikhonhov-derived distance distributions and TR-FRET distance distributions is shown in *SI Appendix*, Fig. S7.

Inspection of the chemical structures of these compounds showed that four of them possess the hallmarks of classical type II DFG-out inhibitors (9) exemplified by the Abl inhibitor imatinib (5), with a "head" group that engages the hinge region of the kinase linking the N- and C-terminal lobes, a "linker" that reaches around the DFG motif, a polar group that hydrogen bonds to the DFG motif and/or catalytic glutamate, and a hydrophobic "tail" group that occupies the hydrophobic back pocket left by the displaced DFG motif (Fig. 5*B*). The type II binding mode has been observed in a relatively small subset of protein kinases, and AurA is not generally considered one of them. However, inspection of an X-ray structure of an analog of AMG-900 from early stages of lead optimization (43) reveals the classical type II binding mode and suggests that the hydrophobic tail group of AMG-900 indeed binds in the hydrophobic back pocket of AurA (Fig. 5*B*). The other putative type II inhibitors were previously reported to be DFG-in binders based on cocrystal structures with AurB (BI-847325 and ZM-447439; Fig. 5*C*) (44, 45) or molecular modeling (GSK-1070916) (46). However, these studies utilized AurB trapped in the DFG-in state by its activator protein INCENP (47). Aligning the AurB:BI-847325 structure (DFG-in) (44) with the structure of AurA bound to the AMG-900 analog (DFG-out) (43) shows that the tail groups of the two compounds superimpose, suggesting that BI-847325 and AMG-900 could bind to similar DFG-out states in AurA (Fig. 5*C*, *Inset*).

To independently confirm the binding modes of these inhibitors, the fluorescent dyes of the FRET sensor were replaced with the paramagnetic spin probe MTSL and the inhibitor-induced conformational changes analyzed using double electron–electron resonance spectroscopy (DEER) (Fig. 5*D*). The DEER results showed that AMG-900 induces a pronounced structural change upon binding to AurA that yields a short spin–spin distance of

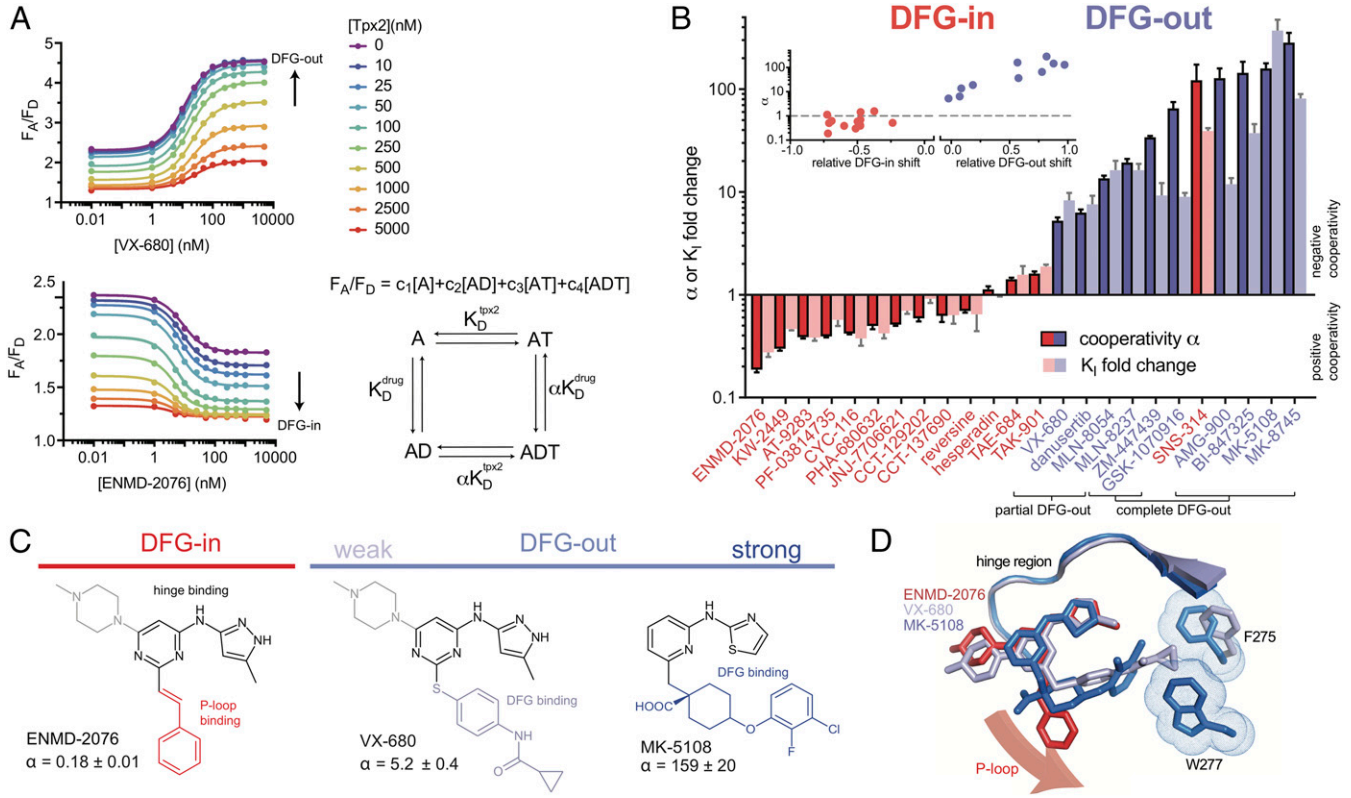

Fig. 6. Inhibitor conformational preferences translate into selectivity for AurA activation states. (*A*) Fluorescence binding data for the DFG-out inducer VX-680 (*Top*) and the DFG-in inducer ENMD-2076 (*Bottom*). The fluorescence signals represent the ratios of the acceptor and donor intensities quantified from emission spectra. Binding data for all compounds are shown in *SI Appendix*, Fig. S8. (*Bottom Right*) The two-site cooperative binding model is shown for Tpx2 (T) and drug (D) binding to AurA (A), consisting of four coupled equilibria described by the indicated equilibrium dissociation constants (K_D values). The cooperativity factor α represents the fold change in the affinity of one ligand in the presence of saturating concentrations of the other. The fluorescence signal F_A/F_D was modeled as a linear function of the concentrations of the four biochemical species, as shown in the indicated equation (*SI Appendix*). (*B*) Cooperativity factors α for the DFG-out (dark blue) and DFG-in (dark red) inhibitors derived from global fitting of the fluorescence binding data, ranked in order of increasing α. Data represent the mean ± SEM; $n = 6$ for the DFG-in inhibitors, $n = 7$ for the partial DFG-out inhibitors, and $n = 4$ for the complete DFG-out inhibitors (*SI Appendix*). The *Inset* shows the α-values as a function of the relative distance shifts toward the DFG-in or DFG-out states derived from the TR-FRET analysis. The faint bars in the main panel represent the fold change in the inhibition constants (K_I) observed in the presence of Tpx2 for each inhibitor. Data represent the mean ± SEM; $n = 3$. (*C*) The chemical structures of ENMD-2076, VX-680, and MK-5108 are shown, with the similar hinge-binding motifs highlighted in black. The cooperativity values are shown for each inhibitor. (*D*) The aligned crystal structures of AurA bound to VX-680 and MK-5108 are shown together with the docked structure of ENMD-2076. The phenylalanine residue of the DFG motif is shown as sticks, and the side chain of W277 in the MK-5108 X-ray structure is shown as dots, highlighting the interactions with the inhibitor.

20 Å, and that the other putative type II inhibitors induce distinct DFG-out states with longer distances ranging from 39 to 43 Å (*SI Appendix*, Fig. S7). In contrast, binding of the DFG-in inducer SNS-314 results in a much longer spin–spin distance of 52 Å, representing a switch to the DFG-in state. These DEER data are in excellent agreement with the FRET measurements (Fig. 5*D*, *Right Inset*, and *SI Appendix*, Fig. S7) and confirm that the putative type II inhibitors indeed bind to AurA in the DFG-out state, not the DFG-in state as reported for AurB. The fact that AMG-900 induces a qualitatively different structural state than the other type II compounds, as reflected in much shorter probe–probe distances (Fig. 5*D*), is likely due to the bulky hydrophobic tail group of AMG-900 causing a larger displacement of the DFG motif than the much smaller tail groups of the other type II inhibitors, resulting in a more dramatic movement of the activation loop across the active site cleft relative to the DFG-in state.

The other two inhibitors that induce unique structural states upon binding to AurA, MK-5108 and MK-8745 (an analog of MK-5108), lack the type II chemical structure, and the X-ray structure of MK-5108 bound to AurA shows that the inhibitor binds to the DFG-out state but interacts only with the edge of the DFG motif without enveloping it (48). Nonetheless, these inhibitors appear to be as efficient at inducing the DFG-out state as the type II compounds, as reflected in the uniformity of the TR-FRET distances observed across all four biochemical states of AurA (Fig. 5*A* and *SI Appendix*, Fig. S4*C*). These results indicate that even type I inhibitors can have strong preferences for the DFG-out state.

Inhibitor Conformational Effects Determine Binding Selectivity for Specific Activation States of AurA. Considering that Tpx2 promotes the DFG-in state and that many of the inhibitors also exhibit pronounced conformational effects, we reasoned that the inhibitors might display either positive or negative binding cooperativity with Tpx2, depending on the direction in which they modulate the DFG equilibrium. To test whether Tpx2 affects the binding affinities of the inhibitors in our panel, binding curves for all 24 compounds were measured using the phosphorylated FRET sensor in the presence of different Tpx2 concentrations. We took two steps to ensure the accurate measurement of cooperativity effects. First, binding was tracked by ratiometric steady-state FRET measurements, in which the ratios of the acceptor-to-donor emission intensities are determined (*SI Appendix*, Fig. S3 *C* and *D*), using a recently developed high-throughput spectral plate reader with sufficient signal/noise to yield excellent emission spectra with 5 nM kinase (49) (Fig. 6*A* and *SI Appendix*, Fig. S8). Second, rather than fitting individual binding curves, the binding cooperativity between inhibitor and Tpx2 was determined directly by globally fitting all fluorescence data for a given inhibitor to the

two-site cooperative binding model shown in Fig. 6*A* using numerical simulation (*SI Appendix*). In this model, the binding cooperativity is described by the cooperativity factor α, which represents the fold change in the inhibitor affinity in the presence of saturating Tpx2. Because of the closed thermodynamic cycle, α is also equal to the fold change in Tpx2 affinity in the presence of saturating inhibitor. Values of α smaller than 1 represent positive cooperativity, and values greater than 1 represent negative cooperativity. Because the binding cooperativity is encoded in the fluorescence data by both the inhibitor dose–responses and the Tpx2 dose–responses, this global fitting approach provides far more accurate determinations of the cooperativity factors than fitting individual inhibitor binding curves.

Remarkably, ranking the inhibitors from lowest to highest α-values segregates them into two groups that, with one exception, correspond to the DFG-in inducers, with small values of α, and the DFG-out inhibitors, with large values of α (Fig. 6*B* and *SI Appendix*, Fig. S9*A*, and Table S2). Ten of the DFG-in inducers have α-values lower than 1, representing positive cooperativity with Tpx2. Within the DFG-out inhibitors, there was a further correspondence between the strength of conformational preference and the magnitude of the cooperativity (Fig. 6*B*, *Inset*), with the partial DFG-out shifters possessing values of α between 5 and 20, and the complete DFG-out shifters (the type II inhibitors and MK-5108/8745) having values of α between 35 and 300. These results indicate that the preference for the DFG-in or DFG-out states is the key driver of inhibitor selectivity for the *Phos* or *Phos+Tpx2* forms of AurA. The one exception is the DFG-in inhibitor SNS-314, which exhibits substantial negative cooperativity with Tpx2. This is explained by the X-ray structure of SNS-314 bound to AurA (33), in which the αC-helix is displaced outwards by the inhibitor, occluding the Tpx2 binding site (*SI Appendix*, Fig. S5*B*).

To independently confirm the cooperativity results, we measured the inhibition constants (K_I values) of all 24 inhibitors using kinase activity assays in the presence and absence of Tpx2. The fold changes in the K_I values in the presence of Tpx2 closely mirrored the α-values (Fig. 6*B*, faded bars, and *SI Appendix*, Fig. S11), providing independent confirmation of the selectivity rankings. These rankings are also consistent with previously published results on a subset of the inhibitors (36, 48, 50, 51). Together, the cooperativity and inhibition data provide a clear picture of the crucial importance of the DFG equilibrium for inhibitor selectivity.

There are several examples in our dataset of molecules that share the same chemical scaffold but differ markedly in conformational selectivity (Fig. 6*C* and *SI Appendix*, Fig. S6 *A* and *B*). A striking example is provided by the four type I inhibitors, ENMD-2076 (DFG-in), VX-680 (partial DFG-out), and MK-5108/MK-8745 (complete DFG-out), all of which share very similar hinge-binding motifs (Fig. 6*C*). Although there is no X-ray structure of ENMD-2076, the binding pose generated by molecular docking superimposes the hinge-binding motif of ENMD-2076 with the corresponding portions of VX-680 and MK-5108 observed in X-ray structures (Fig. 6*D*). Despite the similar structures and binding modes of these inhibitors, their cooperativity factors span three orders of magnitude, demonstrating that conformational preferences can be tuned over a wide range by chemical modifications at a single position on an inhibitor scaffold.

Our results confirm that the type II binding mode is intrinsically specific for the DFG-out state, with all four putative type II inhibitors displaying strong negative cooperativity with Tpx2. In contrast, most type I inhibitors can bind to both the DFG-in or DFG-out states, usually with affinities that differ by less than a factor of 20. Why then are the type I inhibitors MK-5108 and MK-8745 so strongly selective for the DFG-out state? A unique feature of MK-5108 and MK-8745 is that they have very high binding affinity, with K_D values in the low- and mid-picomolar range, respectively. This potency is likely responsible for their unusually strong selectivity for the DFG-out state. The binding data for MK-5108 show that, while this inhibitor binds to AurA more than 100-fold better in the absence of Tpx2, it still binds the AurA:Tpx2 complex with ∼3 nM affinity, more tightly than many of the positively cooperative type I inhibitors. Thus, selectivity for the DFG-out state can arise from a chemical structure that is largely incompatible with the DFG-in state (type II) or simply by binding the DFG-out state with unusually high affinity.

Discussion

An abundance of X-ray structural data have established that some kinase inhibitors, particularly type II compounds, cause substantial structural changes upon binding (5–7). Unfortunately, our understanding of the prevalence of inhibitor-driven structural changes, and how they are linked to binding selectivity, has been limited by the difficulties of quantifying ligand conformational effects in solution. We have filled this gap with a method that tracks kinase structural changes with angstrom-level precision, resolves different conformational states and conformational shifts between states, and is sufficiently scalable to allow large datasets of ligand-induced conformational changes to be rapidly obtained.

Our results provide an unusual glimpse of the ubiquitous nature of inhibitor-driven conformational changes in kinases. Rather than being limited to the type II binding mode, they are a nearly universal feature of ATP-competitive AurA inhibitors. Apparently, AurA is so primed for allostery that essentially any interaction with the active site will alter the conformational ensemble. Importantly, inhibitors with a type I binding mode may promote either the DFG-out or the DFG-in states, and can rival type II inhibitors in their specificity for the DFG-out state.

A second major conclusion is that patterns of inhibitor-induced conformational changes depend strongly on the intrinsic conformational balance of the kinase, resulting in inhibitors with stringent conformational preferences being selective for particular AurA activation states, in some cases to a striking degree. This discovery provides a unifying molecular mechanism for previous reports of Tpx2 affecting the interactions of AurA with inhibitors in vitro (36, 50, 51), and of differential inhibition of functional pools of AurA in cells (48). In particular, MK-5108 and MK-8745 inhibit AurA T288 phosphorylation at the centrosome at low nanomolar concentrations, whereas micromolar concentrations are required to block phosphorylation of some AurA substrates such as Lats2 (48). We have shown that AurA activated only by phosphorylation on T288 is highly dynamic and is maximally sensitive to DFG-out inhibitors like MK-5108/8745, whereas activation of AurA by Tpx2 restrains the kinase in the DFG-in state, rendering it relatively resistant to DFG-out inhibitors. Thus, any cellular readout that depends in part on the Tpx2-bound pool of AurA will be comparatively less sensitive to strong DFG-out inhibitors like MK-5108/8745. Conversely, Tpx2 tends to promote the binding of DFG-in inhibitors. Interestingly, MK-8745 and MK-5108 also show the greatest selectivity for AurA over AurB out of a large panel of inhibitors (48). Since the active sites of AurA and AurB are nearly identical, and AurB function in the cell is dependent on the binding of the Tpx2-like activator INCENP (47), it is likely that the selectivity of inhibitors between AurA and AurB is driven by similar conformational effects.

The ability of inhibitors to differentiate between AurA activation states has potentially important implications for the therapeutic use of these molecules. Differences in the degree to which inhibitors target the various cellular pools of AurA can be expected to translate into distinct therapeutic efficacy and toxicity profiles, depending on the tumor type and genetic background. For instance, roughly 10% of melanoma tumors carry inactivating mutations in the AurA-directed phosphatase PP6C (52, 53). The spindle pool of AurA in these tumor cells is activated by both phosphorylation and Tpx2 (32), and this hyperactivation drives chromosome instability and DNA damage that can be partially reversed by AurA inhibition (54). Our data show that this pathological form of AurA is maximally resistant to DFG-out inhibitors, but that many DFG-in inducers bind preferentially to this form of the kinase and could in principle represent a strategy for treating these melanoma patients. However, our inhibition data show that the fivefold binding preference of ENMD-2076 for the AurA:Tpx2 complex is roughly negated by a similarly lowered K_m

value for ATP (25), highlighting that obtaining 10-fold selectivity for phosphorylated and Tpx2-bound AurA in cells will likely require at least 50-fold binding selectivity. The negative cooperativity of the strong DFG-in inducer SNS-314 highlights that achieving high levels of selectivity will require exquisite complementarity to the rigid active site of the AurA:Tpx2 complex.

Recent studies have shown that AurA plays an important noncatalytic scaffolding role in the pathogenesis of MYCN-amplified cancers, including neuroblastoma and neuroendocrine prostate cancer (NEPC) (18, 55). AurA binds to an N-terminal segment of N-Myc that overlaps with the recognition site of the ubiquitin ligase SCF_{fbxw7}, preventing proteolytic degradation of this oncogenic transcription factor. N-Myc binds across the activation loop of AurA, trapping the kinase in the active DFG-in state (56), and N-Myc binding can be disrupted by DFG-out AurA inhibitors in cells (57, 58), providing a rationale for using DFG-out inhibitors in MYCN-amplified cancers. Alisertib has entered phase 2 clinical trials for both neuroblastoma and NEPC, but early results suggest efficacy is limited (59, 60). Our data reveal that, while alisertib does promote the DFG-out state, this can be negated by a regulatory factor that favors the DFG-in state, suggesting that the ability of alisertib to dissociate the AurA:N-Myc complex in cells will depend on the level of N-Myc overexpression, which differs widely in neuroblastoma patients and correlates with disease progression (61). The type II inhibitor AMG-900, which is a strong DFG-out inducer that triggers an unusually large structural rearrangement upon binding, might be more effective at displacing N-Myc. AMG-900 is currently in early-stage clinical trials for leukemias and solid tumors (62), but to our knowledge has not been tested in a MYCN-overexpressing context.

Protein kinases remain a highly active drug discovery area. In addition to the several dozen kinases for which inhibitors have already received regulatory approval, there is an even larger body of kinase targets with inhibitors in clinical or preclinical development (63). Because the activation loop is the central regulatory structure of all protein kinases, tracking this loop is readily applicable to profiling inhibitor-driven conformational changes in numerous other disease-relevant kinases. Our TR-FRET method provides more detailed structural information than can be obtained using a single environmentally sensitive dye (64), and we anticipate that conformational structure–activity data obtained in this manner could be valuable for guiding the optimization of potency and selectivity during the development of inhibitors for a wide range of targets.

Materials and Methods

Detailed protocols for the following procedures can be found in *SI Appendix*.

Preparation of the FRET Sensor. Protein samples were prepared using a cysteine-light construct of human AurA expressed in BL21-DE3-RIL cells (Agilent) and purified as described (28, 65). Cysteine residues were incorporated at L225 on the D-helix and S284 on the activation loop for labeling with Alexa 488 maleimide (Thermo Fisher) as the donor, and Alexa 568 maleimide as the acceptor. Labeling of donor-only (D-O) and donor-plus-acceptor samples (D+A) was verified by mass spectrometry (*SI Appendix*, Fig. S1 *B* and *C*). A synthetic construct of human Tpx2 (residues 1–43; Selleckchem or Genscript) or a recombinant construct of GST-tagged Tpx2 (residues 1–43) was used for experiments requiring Tpx2.

TR-FRET Fluorescence Assay in 384-Well Plate Format. Plates containing 50-nM FRET sensor +/− inhibitors were read on the fluorescence lifetime plate reader (FLPR). The FLPR is a custom-built instrument designed and built by Fluorescence Innovations. The architecture of the FLPR is shown in Fig. 1*C*. The instrument uses pulsed laser excitation coupled with a high-speed digitizer to measure nanosecond fluorescence decays (31). Instrument response function (IRF) and lifetime measurements were recorded as described in Gruber et al. (66) and Muretta et al. (67).

TR-FRET Data Fitting. Fluorescence waveforms were fit using custom software designed for analysis of time-resolved fluorescence (68) as described by Muretta et al. (69). Briefly, the IRF and the model of fluorescence decay are convolved to describe the measured waveforms. The D+A waveforms were modeled assuming a Gaussian distribution of interfluorophore distances describes the decrease in lifetime compared with the matched D-O sample. The mean distances measured for each inhibitor concentration were fit to the quadratic binding equation in GraphPad Prism to obtain values and confidence intervals for the distances at saturating inhibitor. TR-FRET experiments and fits show excellent consistency across experiments (*SI Appendix*, Fig. S12). Data presented in the main text are from a representative experimental dataset.

Analysis of Binding Cooperativity. The cooperativity analysis was based on ratiometric steady-state fluorescence data collected with the spectral unmixing plate reader (SUPR), a custom-built instrument designed by Fluorescence Innovations. The contributions of the donor and the acceptor to the fluorescence emission were derived by fitting reference spectra for the two dyes and the Raman water band to obtain the spectrally unmixed acceptor/donor ratio (49). Binding data for each inhibitor were globally fit to the thermodynamic model shown in Fig. 6*A* using the numerical simulation program KinTek Explorer (KintekCorp). Data for all inhibitors are shown in *SI Appendix*, Fig. S8.

EPR Experiments. DEER experiments were performed at 65 K using an Elexsys E580 Q-Band spectrometer (Bruker Biospin) as described in *SI Appendix* (68). Data were analyzed using custom software written in Mathematica, which was based on DeerAnalysis 2017 (70).

ACKNOWLEDGMENTS. We thank Joseph Dalluge for help with mass spectrometry, and Greg Gillispie, Benjamin Grant, and Samantha Yuen for technical assistance with fluorescence lifetime measurements. TR-FRET, SUPR-FRET, and DEER experiments were performed at the Biophysical Technology Center, University of Minnesota Department of Biochemistry, Molecular Biology, and Biophysics. This work was supported in part by National Institutes of Health Grant R21 CA217695 (to N.M.L.) and National Institutes of Health Medical Scientist Training Program Grant T32 GM008244 (to E.B.F.).

1. Druker BJ, et al. (2001) Efficacy and safety of a specific inhibitor of the BCR-ABL tyrosine kinase in chronic myeloid leukemia. *N Engl J Med* 344:1031–1037.
2. Paez JG, et al. (2004) EGFR mutations in lung cancer: Correlation with clinical response to gefitinib therapy. *Science* 304:1497–1500.
3. Lynch TJ, et al. (2004) Activating mutations in the epidermal growth factor receptor underlying responsiveness of non-small-cell lung cancer to gefitinib. *N Engl J Med* 350:2129–2139.
4. Manning G, Whyte DB, Martinez R, Hunter T, Sudarsanam S (2002) The protein kinase complement of the human genome. *Science* 298:1912–1934.
5. Schindler T, et al. (2000) Structural mechanism for STI-571 inhibition of Abelson tyrosine kinase. *Science* 289:1938–1942.
6. Pargellis C, et al. (2002) Inhibition of p38 MAP kinase by utilizing a novel allosteric binding site. *Nat Struct Biol* 9:268–272.
7. Wan PT, et al.; Cancer Genome Project (2004) Mechanism of activation of the RAF-ERK signaling pathway by oncogenic mutations of B-RAF. *Cell* 116:855–867.
8. Zhao Z, et al. (2014) Exploration of type II binding mode: A privileged approach for kinase inhibitor focused drug discovery? *ACS Chem Biol* 9:1230–1241.
9. Okram B, et al. (2006) A general strategy for creating "inactive-conformation" abl inhibitors. *Chem Biol* 13:779–786.
10. Fabian MA, et al. (2005) A small molecule-kinase interaction map for clinical kinase inhibitors. *Nat Biotechnol* 23:329–336.
11. Davis MI, et al. (2011) Comprehensive analysis of kinase inhibitor selectivity. *Nat Biotechnol* 29:1046–1051.
12. Carmena M, Earnshaw WC (2003) The cellular geography of Aurora kinases. *Nat Rev Mol Cell Biol* 4:842–854.
13. Hannak E, Kirkham M, Hyman AA, Oegema K (2001) Aurora-A kinase is required for centrosome maturation in *Caenorhabditis elegans*. *J Cell Biol* 155:1109–1116.
14. Seki A, Coppinger JA, Jang CY, Yates JR, Fang G (2008) Bora and the kinase Aurora A cooperatively activate the kinase Plk1 and control mitotic entry. *Science* 320:1655–1658.
15. Macůrek L, et al. (2008) Polo-like kinase-1 is activated by Aurora A to promote checkpoint recovery. *Nature* 455:119–123.
16. Gruss OJ, et al. (2002) Chromosome-induced microtubule assembly mediated by TPX2 is required for spindle formation in HeLa cells. *Nat Cell Biol* 4:871–879.
17. Kufer TA, et al. (2002) Human TPX2 is required for targeting Aurora-A kinase to the spindle. *J Cell Biol* 158:617–623.
18. Otto T, et al. (2009) Stabilization of N-Myc is a critical function of Aurora A in human neuroblastoma. *Cancer Cell* 15:67–78.
19. Dauch D, et al. (2016) A MYC-Aurora kinase A protein complex represents an actionable drug target in p53-altered liver cancer. *Nat Med* 22:744–753.
20. Bischoff JR, et al. (1998) A homologue of *Drosophila* aurora kinase is oncogenic and amplified in human colorectal cancers. *EMBO J* 17:3052–3065.
21. Zhou H, et al. (1998) Tumour amplified kinase STK15/BTAK induces centrosome amplification, aneuploidy and transformation. *Nat Genet* 20:189–193.
22. Joukov V, De Nicolo A, Rodriguez A, Walter JC, Livingston DM (2010) Centrosomal protein of 192 kDa (Cep192) promotes centrosome-driven spindle assembly by engaging in organelle-specific Aurora A activation. *Proc Natl Acad Sci USA* 107:21022–21027.

23. Zorba A, et al. (2014) Molecular mechanism of Aurora A kinase autophosphorylation and its allosteric activation by TPX2. *eLife* 3:e02667.
24. Bayliss R, Sardon T, Vernos I, Conti E (2003) Structural basis of Aurora-A activation by TPX2 at the mitotic spindle. *Mol Cell* 12:851–862.
25. Dodson CA, Bayliss R (2012) Activation of Aurora-A kinase by protein partner binding and phosphorylation are independent and synergistic. *J Biol Chem* 287:1150–1157.
26. Cyphers S, Ruff EF, Behr JM, Chodera JD, Levinson NM (2017) A water-mediated allosteric network governs activation of Aurora kinase A. *Nat Chem Biol* 13:402–408.
27. Gilburt JAH, et al. (2017) Dynamic equilibrium of the Aurora A kinase activation loop revealed by single-molecule spectroscopy. *Angew Chem Int Ed Engl* 56:11409–11414.
28. Ruff EF, et al. (2018) A dynamic mechanism for allosteric activation of Aurora kinase A by activation loop phosphorylation. *eLife* 7:e32766.
29. Levinson NM (2018) The multifaceted allosteric regulation of Aurora kinase A. *Biochem J* 475:2025–2042.
30. Pitsawong W, et al. (2018) Dynamics of human protein kinase Aurora A linked to drug selectivity. *eLife* 7:e36656.
31. Petersen KJ, et al. (2014) Fluorescence lifetime plate reader: Resolution and precision meet high-throughput. *Rev Sci Instrum* 85:113101.
32. Hammond D, et al. (2013) Melanoma-associated mutations in protein phosphatase 6 cause chromosome instability and DNA damage owing to dysregulated Aurora-A. *J Cell Sci* 126:3429–3440.
33. Oslob JD, et al. (2008) Discovery of a potent and selective Aurora kinase inhibitor. *Bioorg Med Chem Lett* 18:4880–4884.
34. Burgess SG, et al. (2016) Allosteric inhibition of Aurora-A kinase by a synthetic vNAR domain. *Open Biol* 6:160089.
35. Janeček M, et al. (2016) Allosteric modulation of AURKA kinase activity by a small-molecule inhibitor of its protein-protein interaction with TPX2. *Sci Rep* 6:28528.
36. Dodson CA, et al. (2010) Crystal structure of an Aurora-A mutant that mimics Aurora-B bound to MLN8054: Insights into selectivity and drug design. *Biochem J* 427:19–28.
37. Bebbington D, et al. (2009) The discovery of the potent Aurora inhibitor MK-0457 (VX-680). *Bioorg Med Chem Lett* 19:3586–3592.
38. Borthakur G, et al. (2015) A phase I study of danusertib (PHA-739358) in adult patients with accelerated or blastic phase chronic myeloid leukemia and Philadelphia chromosome-positive acute lymphoblastic leukemia resistant or intolerant to imatinib and/or other second generation c-ABL therapy. *Haematologica* 100:898–904.
39. Zhao B, et al. (2008) Modulation of kinase-inhibitor interactions by auxiliary protein binding: Crystallography studies on Aurora A interactions with VX-680 and with TPX2. *Protein Sci* 17:1791–1797.
40. Wu JM, et al. (2013) Aurora kinase inhibitors reveal mechanisms of HURP in nucleation of centrosomal and kinetochore microtubules. *Proc Natl Acad Sci USA* 110:E1779–E1787.
41. Fancelli D, et al. (2006) 1,4,5,6-Tetrahydropyrrolo[3,4-c]pyrazoles: Identification of a potent Aurora kinase inhibitor with a favorable antitumor kinase inhibition profile. *J Med Chem* 49:7247–7251.
42. Modugno M, et al. (2007) Crystal structure of the T315I Abl mutant in complex with the Aurora kinases inhibitor PHA-739358. *Cancer Res* 67:7987–7990.
43. Cee VJ, et al. (2010) Discovery of a potent, selective, and orally bioavailable pyridinyl-pyrimidine phthalazine Aurora kinase inhibitor. *J Med Chem* 53:6368–6377.
44. Sini P, et al. (2016) Pharmacological profile of BI 847325, an orally bioavailable, ATP-competitive inhibitor of MEK and Aurora kinases. *Mol Cancer Ther* 15:2388–2398.
45. Girdler F, et al. (2008) Molecular basis of drug resistance in Aurora kinases. *Chem Biol* 15:552–562.
46. Adams ND, et al. (2010) Discovery of GSK1070916, a potent and selective inhibitor of Aurora B/C kinase. *J Med Chem* 53:3973–4001.
47. Sessa F, et al. (2005) Mechanism of Aurora B activation by INCENP and inhibition by hesperadin. *Mol Cell* 18:379–391.
48. de Groot CO, et al. (2015) A cell biologist's field guide to Aurora kinase inhibitors. *Front Oncol* 5:285.
49. Schaaf TM, Peterson KC, Grant BD, Thomas DD, Gillispie GD (2017) Spectral unmixing plate reader: High-throughput, high-precision FRET assays in living cells. *SLAS Discov* 22:250–261.
50. Lavogina D, Enkvist E, Viht K, Uri A (2014) Long residence times revealed by Aurora A kinase-targeting fluorescent probes derived from inhibitors MLN8237 and VX-689. *ChemBioChem* 15:443–450.
51. Anderson K, et al. (2007) Binding of TPX2 to Aurora A alters substrate and inhibitor interactions. *Biochemistry* 46:10287–10295.
52. Hodis E, et al. (2012) A landscape of driver mutations in melanoma. *Cell* 150:251–263.
53. Zeng K, Bastos RN, Barr FA, Gruneberg U (2010) Protein phosphatase 6 regulates mitotic spindle formation by controlling the T-loop phosphorylation state of Aurora A bound to its activator TPX2. *J Cell Biol* 191:1315–1332.
54. Gold HL, et al. (2014) PP6C hotspot mutations in melanoma display sensitivity to Aurora kinase inhibition. *Mol Cancer Res* 12:433–439.
55. Lee JK, et al. (2016) N-Myc drives neuroendocrine prostate cancer initiated from human prostate epithelial cells. *Cancer Cell* 29:536–547.
56. Richards MW, et al. (2016) Structural basis of N-Myc binding by Aurora-A and its destabilization by kinase inhibitors. *Proc Natl Acad Sci USA* 113:13726–13731.
57. Brockmann M, et al. (2013) Small molecule inhibitors of Aurora-A induce proteasomal degradation of N-myc in childhood neuroblastoma. *Cancer Cell* 24:75–89.
58. Gustafson WC, et al. (2014) Drugging MYCN through an allosteric transition in Aurora kinase A. *Cancer Cell* 26:414–427.
59. DuBois SG, et al. (2016) Phase I study of the Aurora A kinase inhibitor alisertib in combination with irinotecan and temozolomide for patients with relapsed or refractory neuroblastoma: A NANT (new approaches to neuroblastoma therapy) trial. *J Clin Oncol* 34:1368–1375.
60. Beltran H, et al. (2018) A phase II trial of the Aurora kinase A inhibitor alisertib for patients with castration resistant and neuroendocrine prostate cancer: Efficacy and biomarkers. *Clin Cancer Res*, 10.1158/1078-0432.CCR-18-1912.
61. Brodeur GM, Seeger RC, Schwab M, Varmus HE, Bishop JM (1984) Amplification of N-myc in untreated human neuroblastomas correlates with advanced disease stage. *Science* 224:1121–1124.
62. Kantarjian HM, et al. (2017) A phase 1 study of AMG 900, an orally administered pan-Aurora kinase inhibitor, in adult patients with acute myeloid leukemia. *Am J Hematol* 92:660–667.
63. Rask-Andersen M, Zhang J, Fabbro D, Schiöth HB (2014) Advances in kinase targeting: Current clinical use and clinical trials. *Trends Pharmacol Sci* 35:604–620.
64. Simard JR, et al. (2009) A new screening assay for allosteric inhibitors of cSrc. *Nat Chem Biol* 5:394–396.
65. Burgess SG, Bayliss R (2015) The structure of C290A:C393A aurora A provides structural insights into kinase regulation. *Acta Crystallogr F Struct Biol Commun* 71:315–319.
66. Gruber SJ, et al. (2014) Discovery of enzyme modulators via high-throughput time-resolved FRET in living cells. *J Biomol Screen* 19:215–222.
67. Muretta JM, et al. (2010) High-performance time-resolved fluorescence by direct waveform recording. *Rev Sci Instrum* 81:103101.
68. Agafonov RV, et al. (2009) Structural dynamics of the myosin relay helix by time-resolved EPR and FRET. *Proc Natl Acad Sci USA* 106:21625–21630.
69. Muretta JM, Rohde JA, Johnsrud DO, Cornea S, Thomas DD (2015) Direct real-time detection of the structural and biochemical events in the myosin power stroke. *Proc Natl Acad Sci USA* 112:14272–14277.
70. Jeschke G, et al. (2006) DeerAnalysis2006—a comprehensive software package for analyzing pulsed ELDOR data. *Appl Magn Reson* 30:473–498.